NRC Research Press

ARTICLE

# Flume investigation of landslide debris–resisting baffles

C.E. Choi, C.W.W. Ng, D. Song, J.H.S. Kwan, H.Y.K. Shiu, K.K.S. Ho, and R.C.H. Koo



**Abstract:** Landslide debris is a common occurrence in mountainous regions around the world that can potentially result in disastrous consequences to downstream facilities. Flow-impeding structures are often constructed along the flow path to impede this hazardous phenomenon. Baffles are a type of flow-impeding structure regularly installed using empirical and prescriptive design methods as the interaction mechanism and the influence of baffle configuration on flow impedance is not well understood. A series of flume experiments were carried out to investigate flows characterizing landslide debris impacting an array of baffles using dry uniform sand. The influence of baffle height, row number, and spacing between successive rows was examined. Photoconductive sensors were used to estimate flow velocity, laser sensors were installed to measure flow depth profiles, and high-speed cameras were used to capture flow kinematics. Experimental results reveal that baffles can be categorized relative to the approach flow depth ($h$) and increasing the baffle height from 0.75$h$ to 1.5$h$ leads to a 40% increase in upstream flow depths from backwater effects, more effective development of subcritical conditions, and additional energy losses of up to 9%. Increasing the number of rows of 1.5$h$ baffles from a single row to a three-row staggered array results in up to 72% additional energy loss. The energy loss is attributed to the deflection of granular jets and additional backwater effects. Increasing the row spacing from 50 to 100 mm results in up to a 14% increase in energy loss.

*Key words:* landslide debris, flume modelling, baffles, array configuration, flow impedance.

**Résumé :** Les débris transportés par les glissements de terrain sont souvent rencontrés dans les régions montagneuses autour du globe, et entraînent des conséquences potentiellement désastreuses aux installations en aval. Des structures pour empêcher les écoulements sont souvent construites le long du chemin d'écoulement pour prévenir ce phénomène dangereux. Les déflecteurs sont un type de structure installés régulièrement selon des méthodes de conception empiriques et prescriptives, puisque le mécanisme d'interaction et l'influence de la configuration des déflecteurs sur la limitation de l'écoulement n'est pas bien compris. Une série d'essais de canaux ont été réalisés pour étudier les caractéristiques d'écoulement des débris de glissement affectés par un groupe de déflecteurs, et ce, à l'aide de sable uniforme sec. L'influence de la hauteur des déflecteurs, du nombre de rangée, et de l'espace entre les rangées successives est évaluée. Des sondes photoconductives ont été utilisées pour estimer la vitesse de l'écoulement, des sondes laser ont été installées pour mesurer les profils de profondeur de l'écoulement, et des caméras à haute vitesse ont été utilisées pour capturer la cinétique de l'écoulement. Les résultats expérimentaux ont révélé que les déflecteurs peuvent être catégorisées selon la profondeur de l'écoulement d'approche ($h$), et que l'augmentation de la hauteur des déflecteurs de 0,75$h$ jusqu'à 1,5$h$ entraîne une augmentation de 40 % de la profondeur de l'écoulement en amont en raison des effets de retour d'eau, un développement plus efficace des conditions subcritiques, et des pertes d'énergie additionnelles jusqu'à 9 %. L'augmentation du nombre de rangées de déflecteurs de 1,5$h$, d'une rangée simple à trois rangées, entraîne une perte d'énergie additionnelle de 72 %. Les pertes d'énergie sont attribuées à la déflection des jets granulaires et aux effets de retour d'eau additionnels. L'augmentation de l'espacement entre les rangées de 50 à 100 mm résulte en une augmentation de 14 % de la perte d'énergie. [Traduit par la Rédaction]

*Mots-clés :* débris de glissement de terrain, modélisation par canaux, déflecteurs, configuration en série, limitation de l'écoulement.

## Introduction

Landslide debris is a type of natural disaster affecting mountainous regions worldwide in Canada (Hungr et al. 2001), Italy (Arattano et al. 2012), Japan (Sassa and Wang 2005), mainland China (Zhang 1993), and Hong Kong (Ho 2004). They travel at high velocities, carry destructive impact energy, and have long runout distances. Countermeasures such as flow-impeding structures are commonly designed along the flow path to impede and retain debris torrents. The use of baffles is particularly effective in impeding mobility for debris flows (Teufelsbauer et al. 2011; Ng et al. 2012), snow avalanches (Hákonardóttir et al. 2001, 2003*a*, 2003*b*; Hauksson et al. 2007), and water outlets in hydraulic engineering (USBR 1987; Roberson et al. 1997; USFHA 2006). The functionality of an array of baffles is to perturb the flow pattern such that flow slows down as it approaches each block, and then accelerates towards the next row to accommodate the dissipation of flow energy upon impact. Figures 1*a* and 1*b* show an array of rectangular baffles installed in front of a rigid barrier (Lantau Island, Hong Kong) and cylindrical baffles installed in an open stream course (Kennedy Town, Hong Kong), respectively. Baffles installed in front of a rigid barrier aim to reduce flow velocity before impact and baffles installed in open stream courses aim to control discharge. In the latter application of baffles, it is imperative to prevent overflow to ensure debris is gradually discharged through the baffles downstream instead of passing uncontrolled over the array of baffles. Baffles are typically designed using empirical or prescriptive approaches as the interaction mechanism and the

Received 25 March 2013. Accepted 4 February 2014.

**C.E. Choi, C.W.W. Ng, and D. Song.** Department of Civil and Environmental Engineering, Hong Kong University of Science and Technology, Clear Water Bay, Kowloon, Hong Kong.
**J.H.S. Kwan, H.Y.K. Shiu, K.K.S. Ho, and R.C.H. Koo.** Geotechnical Engineering Office, Civil Engineering and Development Department, HKSAR.
**Corresponding author**: C.E. Choi (e-mail: cechoi@ust.hk).

**Fig. 1.** Debris flow–resisting baffles: (*a*) installed upstream of barrier (Lantau Islands, Hong Kong); (*b*) installed in open channel (Kennedy Town, Hong Kong).

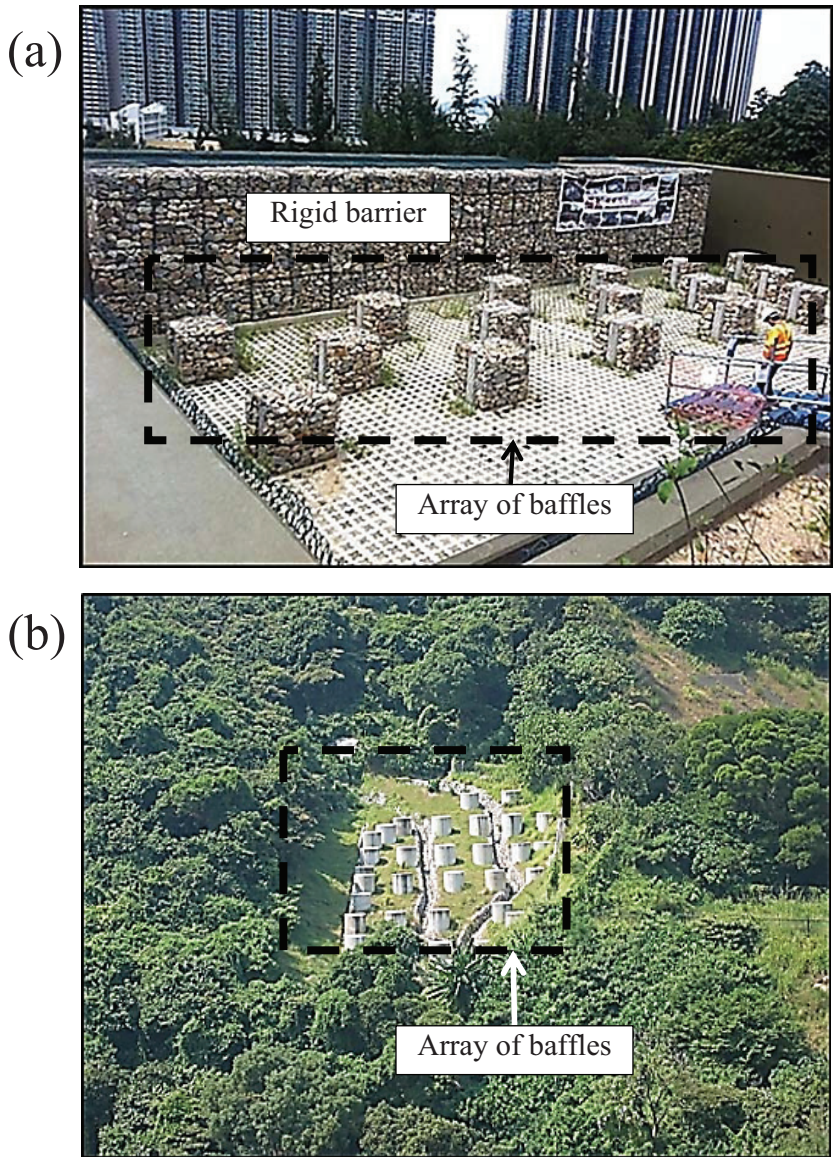




influence of baffle configuration on debris mobility is not well understood.

Flume experiments using granular material have been conducted to model snow avalanche interaction with an array of breaking mounds (Hákonardóttir et al. 2001, 2003*a*, 2003*b*). Experimental results recommend the height of each breaking mound to be taller than the free surface and two times the thickness of the flowing dense core. The aspect ratio of the breaking mound above the free surface should equal unity. Breaking mounds should be placed as close to each other in the transverse direction to promote lateral deflection of jets to further dissipate energy. By encompassing the aforementioned recommendations for snow avalanche breaking mounds, one row of breaking mounds leads to an approximately 20% velocity reduction and a second row of breaking mounds provides an additional 10% velocity reduction (Jóhannesson et al. 2009). However, it is not suitable to adopt snow avalanche recommendations for landslide debris as snow avalanches are characterised by much higher supercritical flow regimes. Landslide debris can be characterised dynamically using lower Froude numbers (i.e., between 0 and 4.5) based on field observations (Arattano et al. 1997; Hübl et al. 2009), whereas snow avalanches are characterised by Froude numbers of about 10 (Hauksson et al. 2007).

Interaction between flowing sediments and obstacles entails complex mechanisms, including the deposition and runup of material behind an obstacle (Chu et al. 1995), formation of dead zones (Faug et al. 2012), granular vacuum (Gray et al. 2003; Zanuttigh and Lamberti 2006), and the deflection of jets between obstacles (Hákonardóttir et al. 2001). These flow mechanisms are distinct for granular flows and cannot be captured by studying the interaction between water and baffles in hydraulic engineering.

Debris flows have complicated rheological behaviour and are dynamically distinct, therefore studies pertaining to snow avalanches and hydraulic engineering are not suitable for application to debris flow–resisting baffles. In this study a series of flume experiments are conducted to examine key flow interaction mechanisms and study the influence of the baffle configuration on flow impedance. The effects of baffle height, number of staggered rows, and spacing between rows are examined.

**Fig. 2.** Flume model.

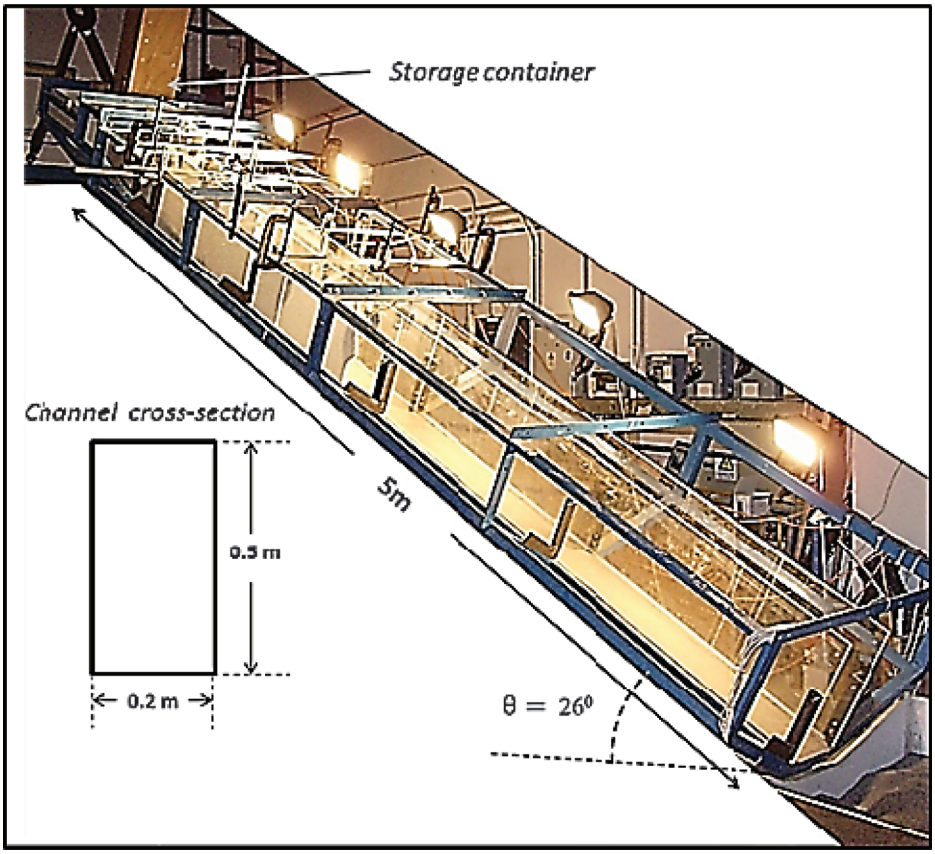


## Flume experiments

### Scaling

Three types of similitude are required for modelling landslide debris baffles, namely (*i*) geometric similarity, (*ii*) kinematic similarity, and (*iii*) dynamic similarity (Chanson 2004). Geometric similarity is achieved by normalizing baffle model dimensions by channel geometry and initial upstream flow conditions. Kinematic similarity describes the impedance resulting from flow interaction, which is unknown and is investigated in this study. Dynamic similarity is attained by adopting the Froude number (*Fr*) that governs the behaviour of gravity driven flows in open channels and interaction with hydraulic structures. The *Fr* number is the ratio of inertial forces to the gravitational forces and is given as follows:

$$(1) \qquad Fr = \frac{v}{\sqrt{gh}}$$

where $v$ is the frontal velocity (m/s), $g$ is the gravitational acceleration (m/s$^2$), and $h$ is the approach flow depth (m). Landslide debris can be characterised with approach *Fr* ranging from 0 to 4.5 based on field observations (Arattano et al. 1997; Hübl et al. 2009). It is acknowledged that flow interaction is highly dependent on the approaching Froude conditions, namely the flow depth and flow velocity at impact (Hübl et al. 2009; Armanini et al. 2011). However, to attain a fundamental understanding of flow interaction between highly complex landslide debris and an array of baffles, an $Fr \approx 3$ is adopted for this study. This characterizes prototype approach velocities of 10 m/s and an approach flow depth of 1 m.

To correct the gravitational component of the Froude number, the following variation of eq. (1) can be adopted:

$$(2) \qquad Fr = \frac{v}{\sqrt{gh\cos\theta}}$$

where $\theta$ is the slope angle (°). The channel inclination used in this study is 26°, hence a correction of the gravitational component will lead to an increase of Froude values by about 7%.

### Flume model

Figure 2 shows a 5 m long rectangular flume (Ng et al. 2012, 2013) with a channel base width ($w$) of 0.2 m and 0.5 m side walls used to investigate the influence of baffle configuration on flow impedance. The channel inclination is set to 26°. The frame encompassing the flume accommodates the mounting and repositioning of lighting and instrumentation. Debris is placed in a storage container located at the most upstream end of the flume. The storage container has a maximum storage volume of 0.08 m$^3$ and is equipped with a spring-loaded door. The spring-loaded door is secured with a magnetic lock. Upon deactivation of the magnetic lock, the spring-loaded door lifts upward and is retained by a hook mechanism at its highest point of accent. A container is placed at the most downstream end of the flume to collect the debris.

### Instrumentation

Ten photoconductive sensors are installed throughout the base of the flume at 0.5 m intervals. Photoconductive sensors are light sensors. When debris passes over each sensor, a signal is sent to the data logger. With the known spacing between photoconductive sensors and the difference in time at which the signal is

received, the average frontal velocity can be deduced. The uncertainty is estimated to be ±0.05 m/s. Laser sensors are mounted overtop of the channel to obtain centreline flow depth measurements perpendicular to the channel base. Flow depth profiles are obtained 100 mm upstream and downstream from the array of baffles. The resolution of the laser sensors is ±4 mm. Two high-speed cameras are used to capture the flow kinematics during interaction. The full resolution capability of the cameras are 768 × 425 pixels and they have a sampling frequency of up to 227 frames per second. One high-speed camera is positioned directly over the array of baffles to capture a plan view of the flow kinematics and approximate the flow velocity at the free surface. Another high-speed camera is positioned on the side of the flume to capture side flow kinematics and obtain flow depth measurements.

## Test programme

Details of 10 tests consisting of a control test and nine different baffle configurations are summarized in Table 1. The baffle heights were selected relative to the approach flow depth ($h$) and details on the approach flow depth are discussed later. The three baffle heights studied were 0.75$h$ (60 mm), $h$ (80 mm), and 1.5$h$ (120 mm). The number of rows was varied from one to three for baffle heights of 0.75$h$ and 1.5$h$. Two different row spacings were studied, 50 mm (0.25 times the width of the channel) and 100 mm (0.5 times the width of the channel). Full and half baffles were used to form staggered formations that are more effective in disrupting streamlines (USFHA 2006). To ensure landslide debris baffles (provide impedance through perturbing flow path) are modeled instead of slit dams (retain flow volume), transverse blockages of less than 40% are selected, based on empirical criteria that fall outside design recommendations for landslide debris slit dams (Watanabe et al. 1980; Ikeya and Uehara 1980). The slit opening ($b$) is normalized by the maximum particle size ($d_{max}$) and should fall outside the range of the following relationship proposed by Watanabe et al. (1980):

$$b / d_{max} < 2.0 \quad (3)$$

Furthermore, the ratio of the summation of slit openings across the width of the channel over the channel width ($B$) should fall outside the range of the following relationship proposed by Ikeya and Uehara (1980):

$$\sum b / B = 0.2 \sim 0.6 \quad (4)$$

A one-dimensional representation of obstruction (independent of the baffle height) along the transverse direction can be characterised by the degree of transverse blockage ($T_b$) and is given as follows:

$$T_b = (b / w) \times 100 \quad (5)$$

where $b$ is the sum of each baffle width along the transverse direction and $w$ is the channel width. For the array to be acting as baffles instead of a slit dam, the array must be less than an equivalent of 40% transverse blockage (Ikeya and Uehara 1980; Watanabe et al. 1980).

Figure 3 shows a plan view of the baffle configurations and an enlarged front view of an individual baffle. The plan dimension for individual baffles with 30% transverse blockage are 20 mm × 20 mm for full baffles and 20 mm × 10 mm for half baffles to accommodate staggered formations. For 30% transverse blockage, each row of baffles occupied 60 mm of the 200 mm channel.

**Table 1.** Summary of baffle configurations.

| Test ID* | Baffle height, $H$ | Number of rows | Spacing between successive rows (mm) |
|---|---|---|---|
| H0_R0 | 0 | 0 | — |
| H075_R1 | 0.75$h$ | 1 | — |
| H075_R2_L5 | 0.75$h$ | 2 | 50 |
| H075_R2_L10 | 0.75$h$ | 2 | 100 |
| H075_R3_L10 | 0.75$h$ | 3 | 100 |
| H1_R1 | $h$ | 1 | — |
| H15_R1 | 1.5$h$ | 1 | — |
| H15_R2_L5 | 1.5$h$ | 2 | 50 |
| H15_R2_L10 | 1.5$h$ | 2 | 100 |
| H15_R3_L10 | 1.5$h$ | 3 | 100 |

**Note:** $h$, approach flow depth.
*H is the baffle height; R is the number of rows used; L is the spacing between successive rows.

## Model preparation and test procedure

To understand the complex fundamental flow mechanisms, it is imperative to first understand the simplest flow cases by using dry granular materials. Therefore, dry Leighton Buzzard Fraction C sand was used in this study. Leighton Buzzard Fraction C sand composes of fairly uniform grains with diameters between 300 and 600 μm. A flow mass of 100 kg was used for all experiments and the initial bulk density in the storage container was maintained at 1680 kg/m³. The interface friction angle between the sand and the plastic film was measured in the laboratory using the method described by Savage and Hutter (1989). Leighton Buzzard Fraction C sand was placed into a paper cylinder on the flume base. The flume was inclined until the paper cylinder began sliding. The interface friction angle was measured as 22.6°.

Each test is setup by installing individual aluminium baffles with dual screws (see Fig. 4) perpendicularly onto the base of the channel to form the appropriate configuration. Dual screws are used to prevent rotation and ensure rigidity during the flow process. Plastic film is then used to cover the top of each full baffle to prevent sand from depositing inside the opening for the screws. Half baffles are plastered onto the side channel wall with double-sided adhesive to ensure rigidity and that no sand passes through its interface with the channel side wall. The first row of baffles is positioned 800 mm downstream from the storage container door. Once the baffles are installed, two high-speed cameras are mounted to obtain a suitable plan and elevation view for high-speed imagery analysis. 500W lamps are adjusted along the flume to ensure lighting is appropriate for high-speed imagery.

The storage container door is closed and secured by activating the magnetic lock. Two springs attached to the storage door are loaded. The systematic layering of 100 kg of sand is conducted within the storage container to reach the target bulk density of 1680 kg/m³. Once the sand is prepared, the flume is gradually inclined to 26° and all the instrumentation is connected to the data logger. The spring loaded storage door is released upon deactivation of the magnetic lock and the door is caught by a hook mechanism at its highest point of accent to allow the sand to freely flow outside of the storage container. The data logger records measurements at 10 000 Hz synchronously as the storage door opens. Debris propagates downslope through the zone of baffles and continues into a collection container at the most downstream end of the flume.

### High-speed imagery

The flow velocity of highly transient and surge like debris flows are difficult to estimate regardless of the instrument or method used (Hákonardóttir et al. 2001; Arattano and Franzi 2003). It is reported that the uncertainty associated with estimating flow velocity using high-speed imagery can be ±0.5 m/s even at

**Fig. 3.** Plan view of baffle array and enlarged front view of baffle (all dimensions in millimetres).

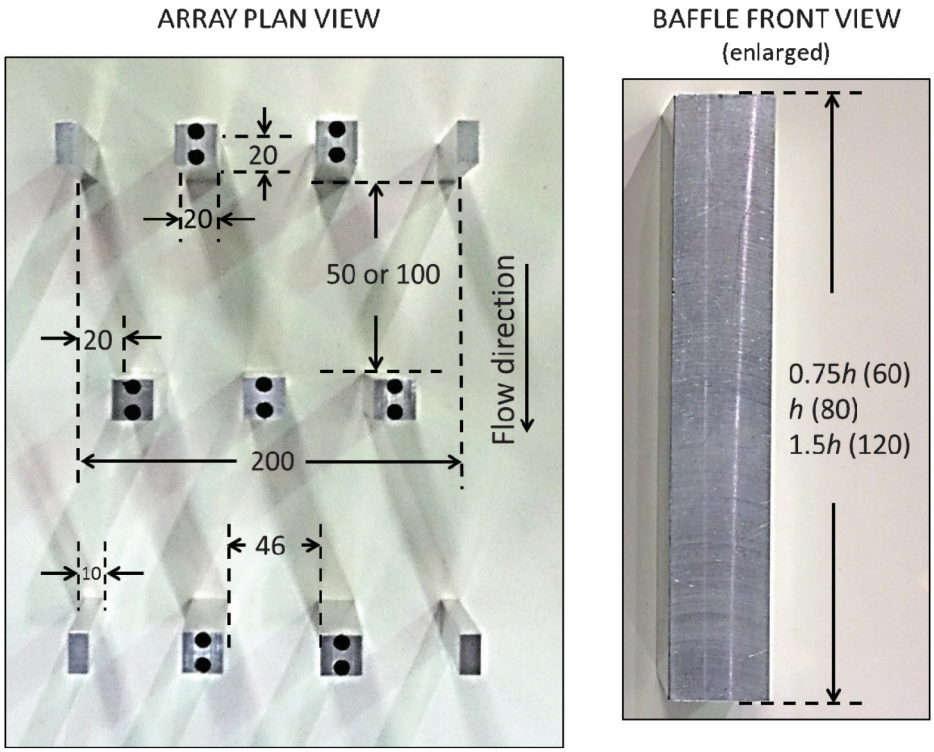


**Fig. 4.** Plan view of instrumentation setup.

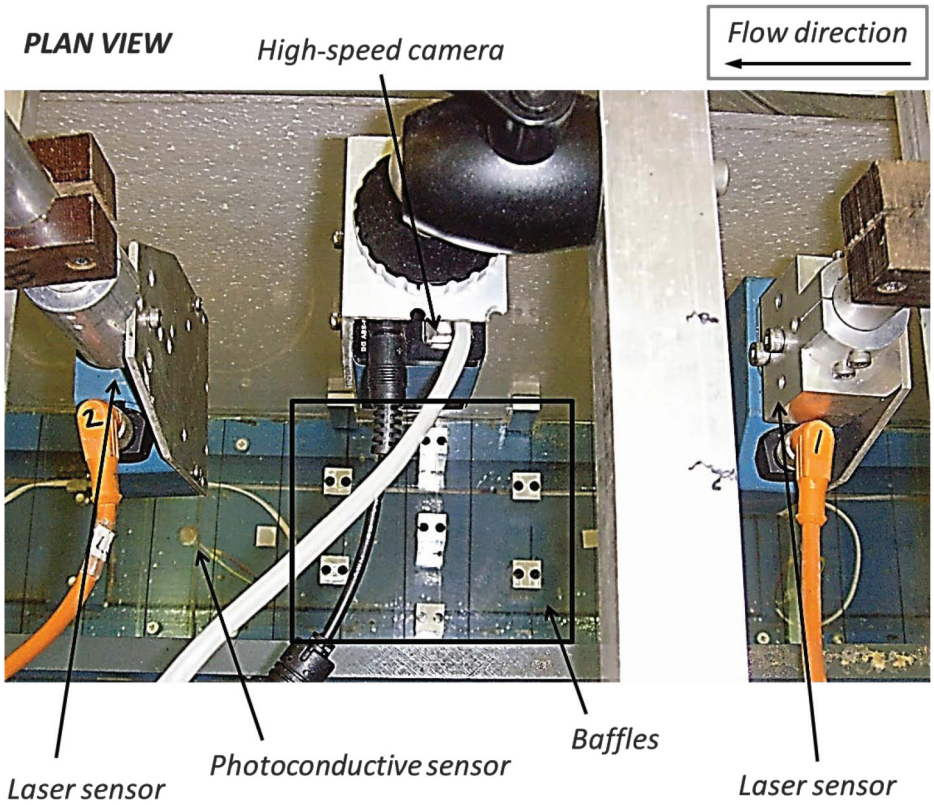


250 frames per second (Hákonardóttir et al. 2001). The particle tracing techniques where two frames for high-speed imagery are compared to trace darker particles is commonly adopted in granular flow problems (Hákonardóttir et al. 2001, 2003*a*; Hauksson et al. 2007; Favier et al. 2009). The particle tracing technique was reported by Hauksson et al. (2007). Two sets of images are compared to track distinct darker tracer particles with a reference grid to estimate the displacement. To facilitate the velocity estimate and

**Fig. 5.** Particle tracking of dark tracer particles with reference grid.

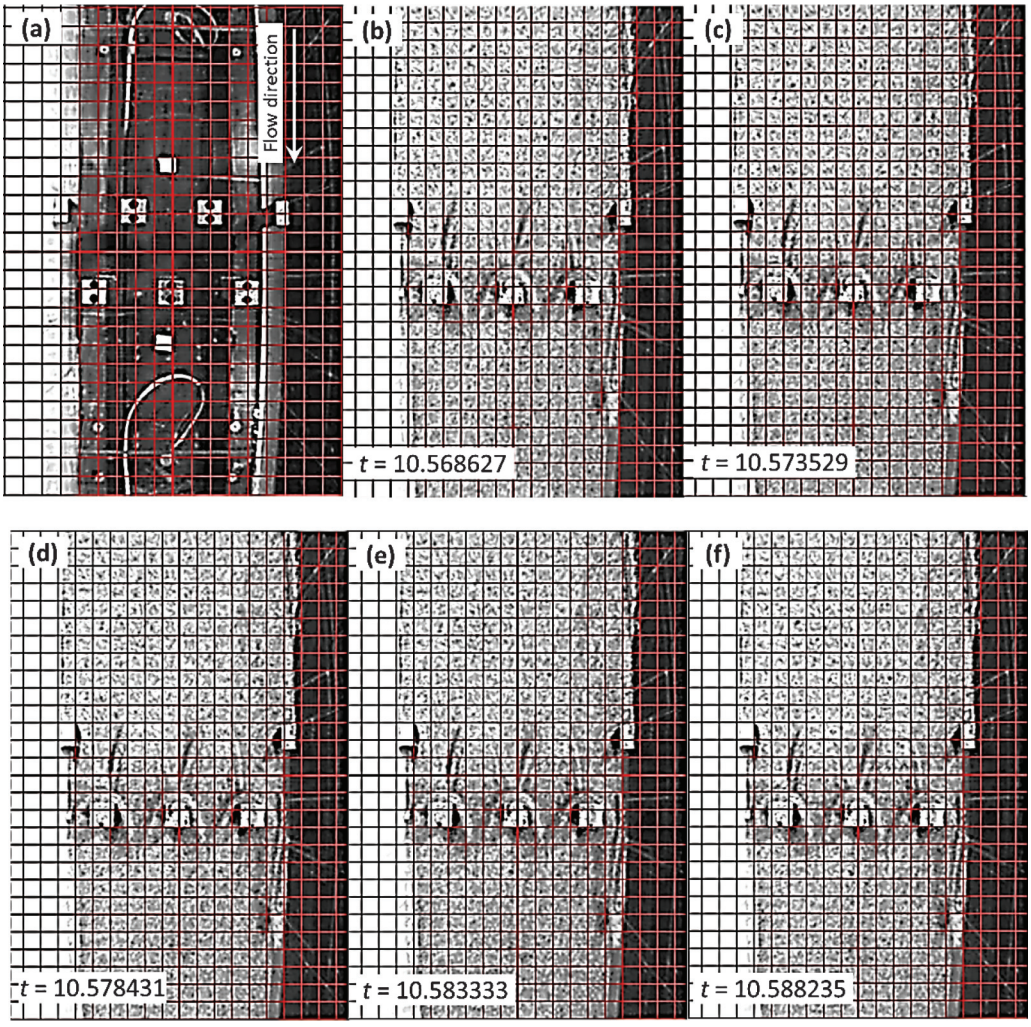


measurements, 15% of the sand was dyed black for particle tracing in this study. High-speed camera image analysis was conducted by placing a reference grid on each image as shown in Fig. 5. Each image is corrected for distortion before analysis and brightness to facilitate particle tracking. Figure 5*a* shows a typical plan view of an array of baffles after distortion correction and placing a grid on the image. Figures 5*b* through 5*f* show how individual particles between several sets of images can be tracked. Combining the displacement over a known time interval, the average velocity of the particles around the baffles can be deduced. It is acknowledged that the free surface velocity may not be coherent with flow velocity along the debris thickness and dead zones cannot be captured.

## Energy principle

The conservation of energy within a control volume is used to estimate the impedance resulting from a particular array of baffles. For simplicity, it is assumed that the compressibility of the flow does not change significantly during the flow process and the surface velocity is taken to characterize the kinematics of the flow. The control volume extends 100 mm upstream from the first row of baffles and 100 mm downstream from the last row of baffles. The flow energy entering the control volume upstream of the baffles is given as $E_u$. The energy of the flow leaving the control volume downstream of the baffles is given as $E_d$. The energy loss associated with the impedance provided by the baffles is given as $\Delta E$. The control volume is shown in Fig. 6. The Bernoulli's energy equation within a control volume is given as follows:

$$E_u - E_d - \Delta E = 0 \quad (6)$$

$$\left(h_u + \frac{v_u^2}{2g} + z_u\right) - \left(h_d + \frac{v_d^2}{2g} + z_d\right) - \Delta E = 0 \quad (7)$$

where $z_u$ is the potential head at upstream monitoring station (m), $z_d$ is the potential head at downstream monitoring station (m), $h_u$ is the upstream flow depth (m), $h_d$ is the downstream flow depth (m), $v_u$ is the upstream flow velocity (m/s), $v_d$ is the downstream flow velocity (m/s), and $g$ is the acceleration due to gravity (m/s$^2$).

## Interpretation of experimental results

### Control test

A series of calibration experiments were conducted without baffles to determine the appropriate location along the flume where dynamic similiarity could be achieved, or in other words, where to place the first row of baffles. The location along the flume, channel inclination, and source volume are variables influencing the Froude number. It was determined that the appropriate location along the flume to achieve dynamic similarity was 800 mm from the storage container door. Details of the control test results were reported in Ng et al. (2012) and flow depth and

**Fig. 6.** Side view of monitoring sections (all dimensions in millimetres).

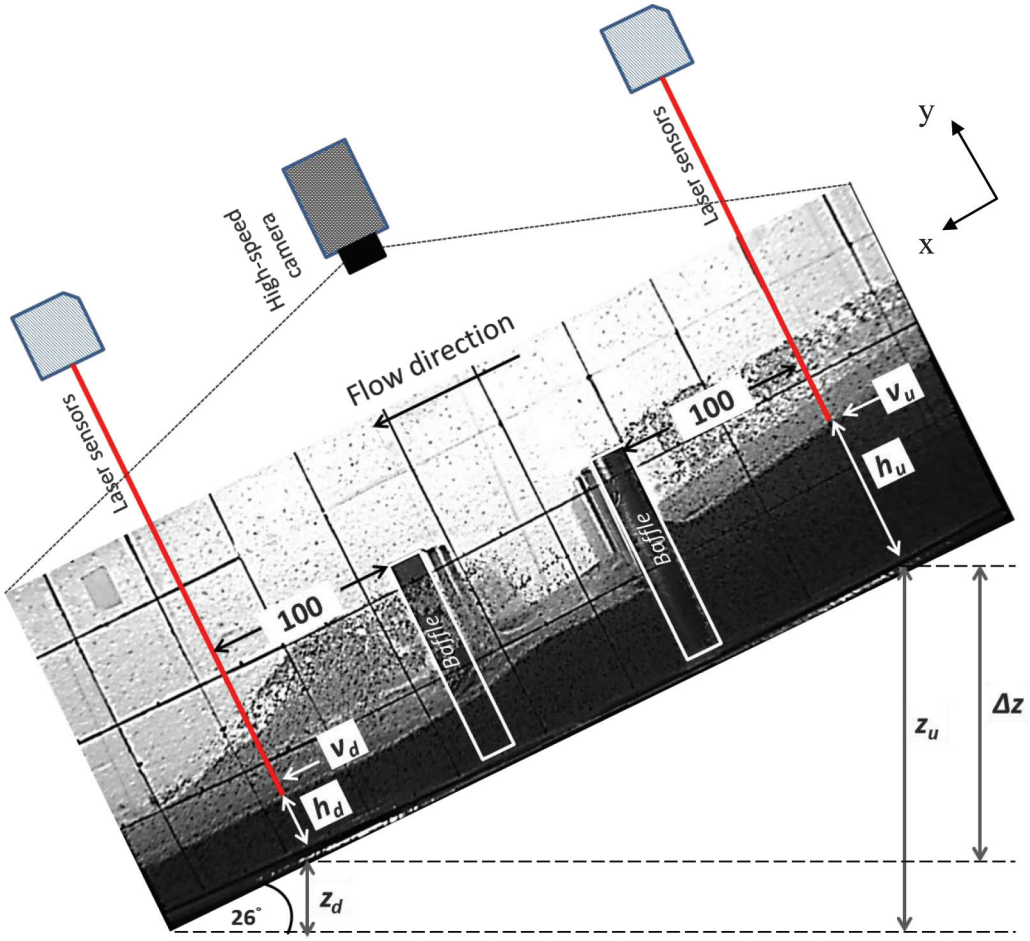


frontal velocity measurements are shown for brevity. Figure 7 shows a comparison of flow depth profiles measured from a laser sensor and captured using the side high-speed camera. The location of measurement is 800 mm downstream from the storage container door. Figure 8 shows frontal velocity profiles estimated from photoconductive sensors along the normalized distance along the entire flume ($N_d$). Three tests are conducted to demonstrate the repeatability of the results. The approach frontal velocity ($v$) 800 mm downstream from the storage container door is approximately 2.7 m/s. Coupling the frontal velocity with the flow depth 800 mm from the storage container, $Fr \approx 3$ is achieved.

## Observed flow kinematics

The interaction process can be characterised by two major regimes, transient state regimes where the flow kinematics are highly incoherent and quasi-steady state regimes where the flow is relatively coherent. During quasi-steady state regimes, the flow depth has receded below the baffle height and transient state kinematics are no longer observed. Figure 9 shows typical transient state flow kinematics for interaction of supercritical granular flow through an array of rigid rectangular baffles. The flow front rapidly propagates downslope and remains laterally uniform prior to impinging the array of baffles (see Fig. 9*a*). The flow front impacts the first row of baffles and flow thickness or shocks (Cui et al. 2007; Gray and Cui 2007) are observed in the region around the baffles. As debris propagates through the first row of baffles, the flow diverges into three granular jets (see Fig. 9*b*). The granular jets impact the second row of staggered baffles, while runup and deposition simultaneously occurs upstream of the first row (Chu et al. 1995; Gray et al. 2003). A relatively symmetrical deflection pattern is observed between the baffles as granular jets deflect laterally into each other to promote additional energy dissipation. As debris weaves through the array, granular jets divide into six thinner jets as flow moves past the second row (see Fig. 9*c*). Upstream of the first row, runup eventually exceeds the baffle and dispersed airborne particles are observed. Granular jets continue to deflect through the staggered array (see Fig. 9*d*) and once airborne particles subside, overflow begins cascading over the first row. Granular jets in between baffles continue to increase in thickness (see Fig. 9*e*) and a granular void is observed in between successive rows. Overflow continues to cascade over the array of baffles and engulfs the second row (see Fig. 9*f*).

## Influence of baffle height

### *Upstream flow depth*

Figure 10 shows a comparison of upstream flow depth profiles and the influence of varying the baffle height. Single row arrays with heights of 0.75$h$ (test H075_R1), $h$ (test H1_R1), and 1.5$h$ (test H15_R1) are compared. For upstream comparisons, the time is taken as $t = 0$ s when the flow front is about to enter the array of baffles and subsequent flow interaction is captured for 20 s. Flow depths are normalized against the approach flow depth ($h$) of 80 mm. Three horizontal reference lines are shown for each baffle height investigated. In addition, a control test (H0_R0) is shown for reference. The control test (H0_R0) rapidly increases to the approach flow depth ($h_u/h = 1$) before gradually attenuating for the remainder of the captured flow process. Flow interacting with 0.75$h$ baffles (test H075_R1) exhibits a 20% increase in peak flow depth compared to the control test before decreasing to 0.3 times

**Fig. 7.** Comparison of flow depth measurements 800 mm downstream from storage container for control test.

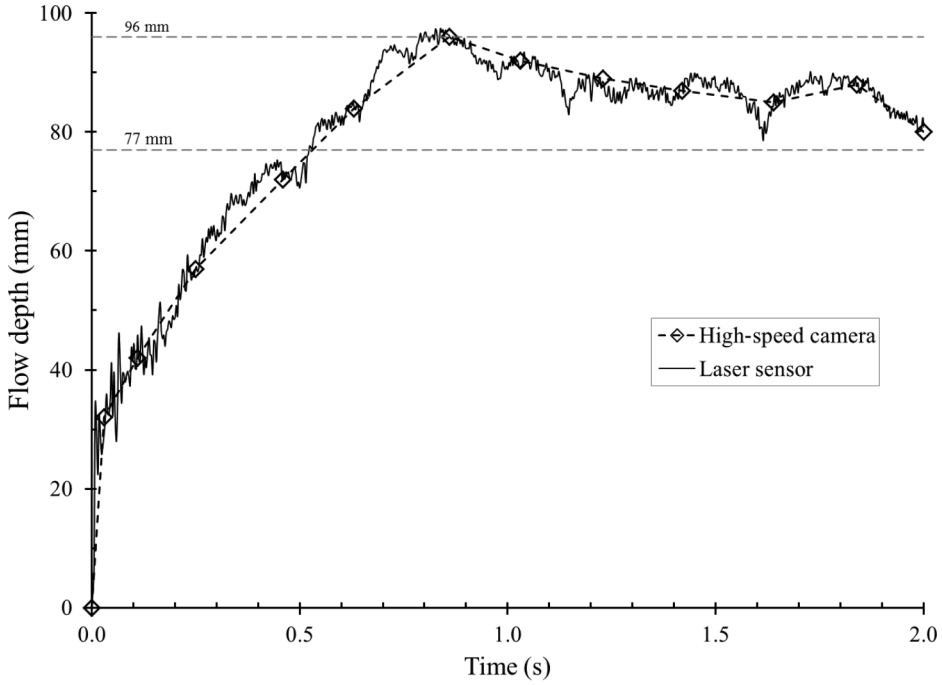


**Fig. 8.** Comparison of frontal velocity profiles.

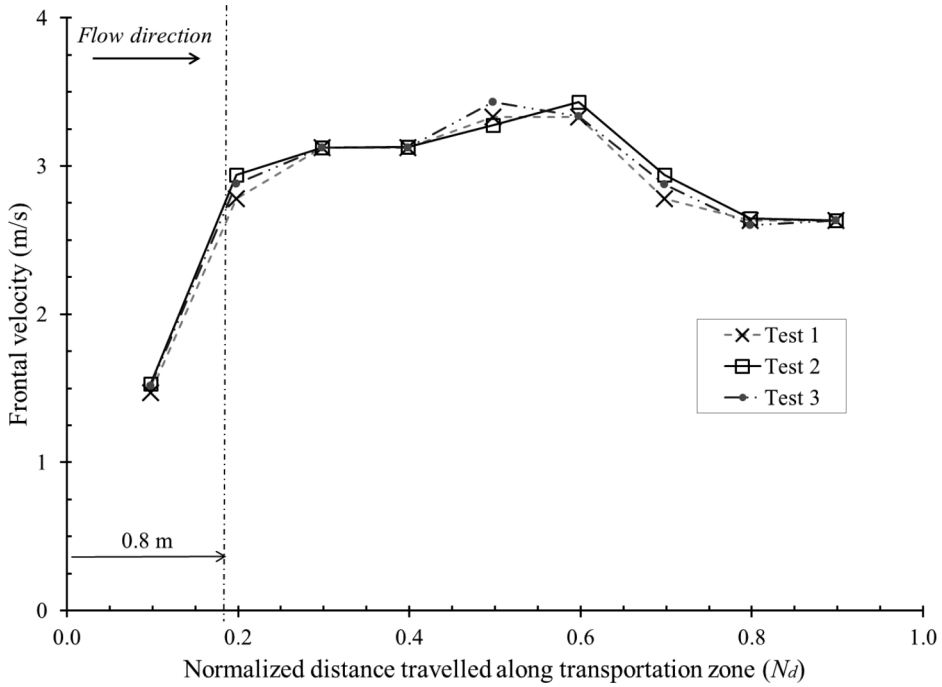


the approach flow depth at $t = 10$ s and remaining relatively stable for the remainder of the captured flow process. Likewise, flow interaction with $h$ baffles (test H1_R1) exhibits similar behaviour as the $0.75h$ tall array and a 10% increase in peak upstream flow depth compared to the control test. Finally, the $1.5h$ baffles (test H15_R1) exhibit a 60% increase in peak flow depth compared to control test conditions. Increasing the baffle height from $0.75h$ to $1.5h$ leads to an increase in peak upstream flow depth from backwater effects by up to 40%.

The increase in upstream flow depth resulting from baffles is reminiscent of the concept of backwater in hydraulic engineering when choking occurs between two bridge piers. Choking develops when there is a change in bed elevation or channel width and is defined as the threshold constriction that will lead to critical flow conditions at the constriction (Jain 2001). Choking will lead to increase in upstream flow depth and minimum energy discharges through the constriction. Although the concept borrowed from hydraulic engineering may not entirely be applicable for transient surge granular flow because of the development of stagnant regions directly upstream of the baffles (Chu et al. 1995; Cui et al. 2007; Gray and Cui 2007), the concept of choking may serve as a preliminary assessment on whether overflow will occur if the

**Fig. 9.** Flow kinematics (test H15_R2_L10): (*a*) $t$ = 0 s; (*b*) $t$ = 0.035 s; (*c*) $t$ = 0.075 s; (*d*) $t$ = 0.170 s; (*e*) $t$ = 0.357 s; (*f*) $t$ = 0.490 s.

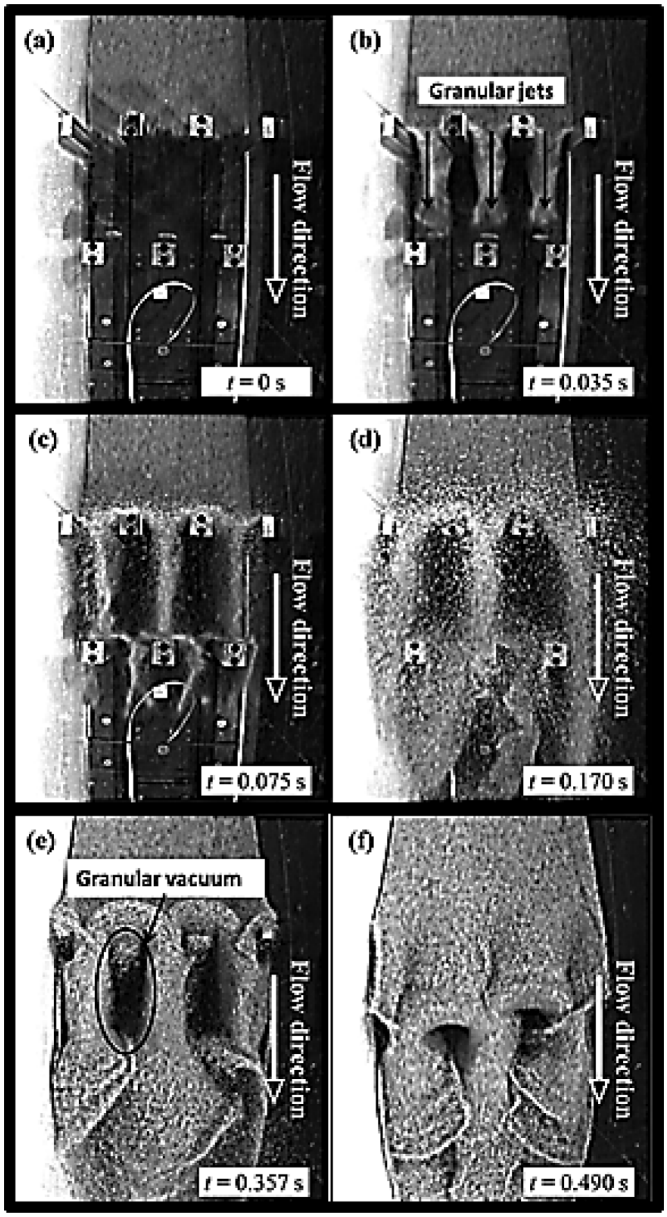


medium is treated as a Newtonian fluid. Overflow is only an important phenomenon to consider when baffles are used on open hill slopes as discharge controlling structures (see Fig. 1*b*). A simple back-of-envelope calculation is conducted. The tallest baffle used in this research is 1.5$h$ or 0.12 m and the debris is assumed to be Newtonian in nature for simplicity. The input energy based on Froude scaling ($Fr \approx 3$) has an approach flow depth of 80 mm and an approach velocity of about 2.7 m/s. Combining the initial approach flow depth and velocity leads to a specific energy of about 0.45 m. In order for choking and backwater to occur, the approach specific energy must be less than the specific energy required for choking. The specific energy for choking is deduced by summing the height of the baffle (0.12 m) and the critical specific energy. The critical specific energy is estimated using the critical depth for rectangular channels which is calculated using $h_c = (q^2 / g)^{1/3}$, where $q$ is the discharge per unit width and $h_c$ is the critical depth. Furthermore, the critical specific energy is also the minimum specific energy and is deduced using the relationship $E_{critical}$ = 1.5$h_c$, and is calculated as 0.17 m. The specific energy required for choking is thus 0.29 m and is significantly less than the approach specific energy of 0.45 m. Hence, choking and subsequent backwater or overflow should not occur, however overflow processes are observed in the experiments. This implies that the hydraulic theory pertaining to backwater resulting from bridge piers is not entirely applicable to debris flow baffles because of the presence of stagnant zones promoting overflow (Cui and Gray 2013) and possibly some degree of dynamic arching in the slits (Vreman et al. 2007).

Overflow is only an important phenomenon to consider when baffles are used on open hill slopes as discharge controlling structures (see Fig. 1*b*). The difference in flow depth between the peak flow depth resulting from each baffle array and its corresponding reference line characterizes the potential overflow that may occur during flow interaction. Results reveal that baffles shorter than the approach flow depth lead to greater potential overflow, whereas baffles taller than the approach flow depth are more effective in suppressing overflow. The suppression of overflow is important as it travels over an array of baffles unimpeded and can discharge at high energies downstream (Jóhannesson et al. 2009). Supercritical overflow is particularly hazardous in situations where its trajectory cannot be easily predicted. Jóhannesson (2001) surveyed a torrent which had been deflected by a dam at Flateyri in northwestern Iceland and observed that the deflected stream came to rest 100 m further downslope than the undeflected part. Overflow requires careful consideration in the design of flow-impeding structures.

### *Upstream Froude number*

Figure 11 shows a comparison of upstream Froude conditions and the influence of varying the baffle height. A reference line for critical conditions is shown ($Fr \approx 1$). Since the flow front is wedge shaped, the Froude number at the tip is theoretically infinity. Hence the control test (H0_R0) without baffles initially exhibits a relatively high Froude number ($Fr \approx 6$) 100 mm upstream from the first row of baffles just as the flow front enters the baffles ($t$ = 0 s). As the flow front propagates downstream, the flow thickness increases and the Froude number sharply drops to the target initial upstream condition ($Fr \approx 3$). Flow conditions remain supercritical until $t$ = 4 s where transition into the subcritical regime is observed. Flow interaction with 0.75$h$ baffles (test H075_R1) exhibits a similar sharp reduction in supercritical flow conditions upon impacting the baffles ($Fr \approx 2.5$) and develops critical conditions just after $t$ = 17 s. Likewise, a single row of $h$ baffles (test H1_R1) and 1.5$h$ baffles (test H15_R1) exhibit rapid attenuation of supercritical flow upon impact. As the baffle height is increased from 0.75$h$ to $h$, more effective suppression of supercritical conditions is observed between $t$ = 0 and 2 s. However, increasing the baffle height from $h$ to 1.5$h$ does not exhibit an obvious improvement in suppression of supercritical conditions. Results correspond accordingly to hydraulic engineering, where increasing the height of the obstruction at the base of the channel relative to the critical flow depth will lead to more effective development of a hydraulic–granular jump. A hydraulic–granular jump will lead to more effective dissipation of flow energy upstream of the baffles as shallow and fast moving supercritical granular flow impacts deep and slow granular flow immediately upstream of the baffles.

### *Energy loss*

Figure 12 shows a comparison of energy loss profiles ($\Delta E/E_a$) between 0.75$h$ and 1.5$h$ baffles. The energy loss ($\Delta E$) is normalized with initial upstream approach energy ($E_a$). This initial approach energy is the same for all tests and selected based on dynamic similarity ($Fr \approx 3$). The normalized energy loss ($\Delta E / E_a$) characterizes the impedance resulting from an array of baffles relative to the initial approach energy before impact. Single row and three row arrays for 0.75$h$ and 1.5$h$ baffles and a control test without

**Fig. 10.** Comparison of upstream flow depth and overflow for varying baffle heights.

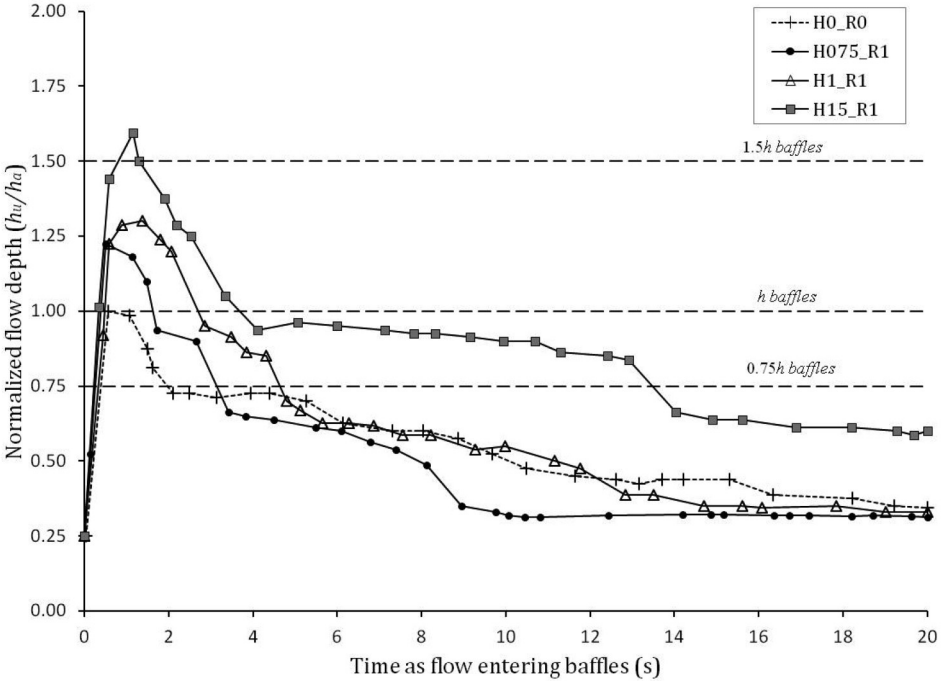


**Fig. 11.** Comparison of upstream Froude conditions for varying baffle heights.

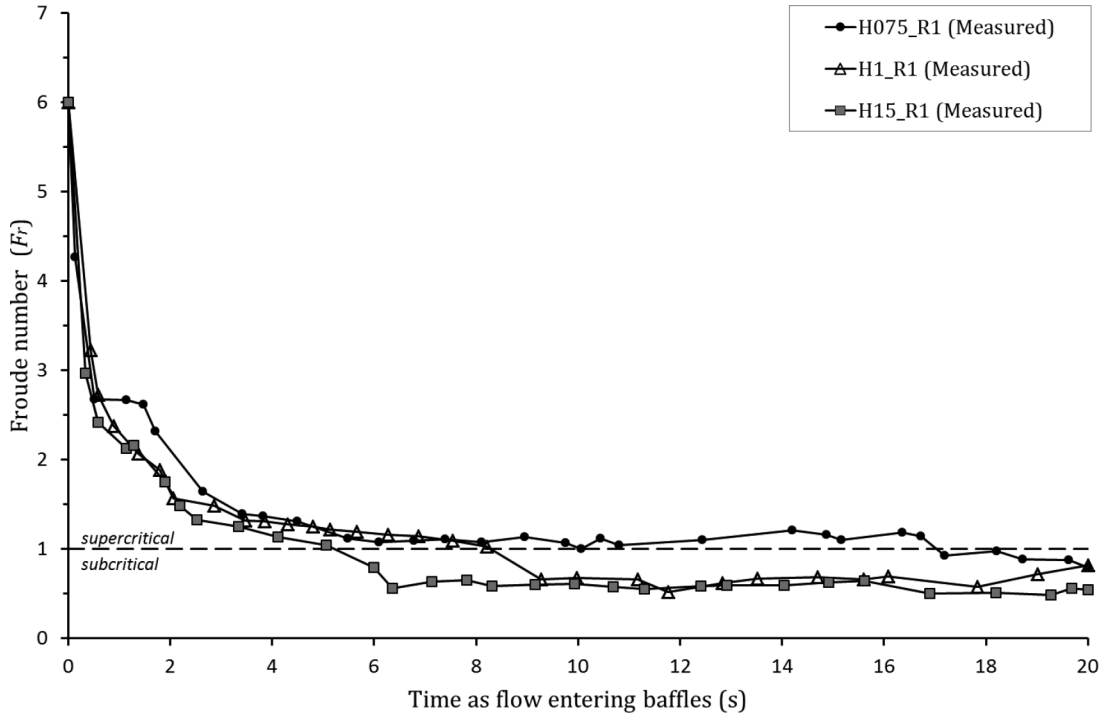


obstruction within the channel are compared. Each energy loss profile exhibits a sharp loss in energy once flow is observed exiting the control volume. The sharp energy loss is characterized as the transient state flow regime where the flow is highly incoherent and flow kinematics of overflow and granular jets are observed. The transient state energy loss occurs within a small time interval of approximately less than $t$ = 2 s. After the transient state, a gradual stabilization of energy loss is observed and this regime is characterised as the quasi-steady state regime.

The control test (H0_R0) exhibits a peak in energy reduction as the flow front exits the control volume and is followed by a quasi-steady energy loss from elevation and frictional losses. Results reveal that arrays of 1.5$h$ baffles exhibit greater energy loss compared to arrays of 0.75$h$ baffles during the transient state regime and the influence of baffle height is not substantial as flow enters into quasi-steady state flow. A single row array of 1.5$h$ baffles (test H15_R1) leads to 7% more energy loss during the initial stages of interaction compared to a single row array of 0.75$h$ baffles. A

**Fig. 12.** Comparison of energy loss and baffle height.

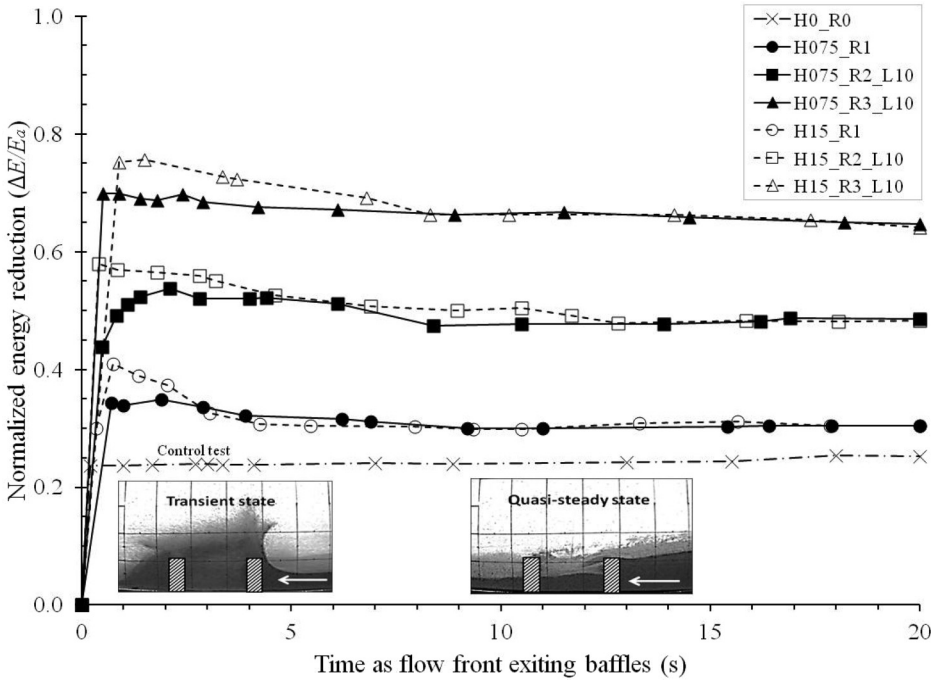




comparison of both two and three row arrays with heights of 0.75*h* and 1.5*h* reveal that 1.5*h* baffles lead to energy loss increases of 9% and 7%, respectively. It is evident from a comparison of 0.75*h* with 1.5*h* baffles that taller baffles exhibit greater impedance during the transient state compared to shorter baffles and the influence of baffle height is negligible during the quasi-steady state flow regime.

The difference in energy loss between tall (1.5*h*) and short (0.75*h*) baffles is because (*i*) the dissipation of potential and kinetic energy through the suppression of runup along a taller baffle face, (*ii*) unobstructed overflow is suppressed with the use of taller baffles, and (*iii*) taller baffles are more effective at developing subcritical upstream conditions which potentially lead to the development of hydraulic/granular jumps (see Fig. 11). Once the flow depth entering the control volume recedes below the height of the 0.75*h* baffles, the influence of baffle height is no longer significant, thus the energy loss profiles comparing baffle height exhibit negligible difference at quasi-steady state flow. The results are consistent with recommendations by Hákonardóttir et al. (2001), where it is reported that obstacles must remain higher than that of the flow depth for obstacles to remain effective and not buried by the flowing medium and Jóhannesson et al. (2009) state that if obstacles are not high enough, supercritical overflow will discharge downstream resulting in potential hazard.

## Influence of additional rows

### *Upstream flow depth*

Figure 13 shows a comparison of normalized upstream flow depth profiles and the influence of varying row arrangements. The row number is increased from a single row to three staggered rows. A reference line is shown for a baffle height of 1.5*h* and the control test is shown for reference. Increasing the number of rows of baffles from a single row array (test H15_R1) to two staggered rows spaced 100 mm apart (test H15_R2_L10) leads to a negligible increase in peak upstream flow depth and further placing a third staggered row to impede the flow (test H15_R3_L10) at the same longitudinal spacing of 100 mm leads to 11% increase in peak upstream flow depth. The area underneath the upstream flow depth profile and the reference line characterizes the extent of backwater effects and potential overflow. It is evident from upstream flow depth profiles that as the number of rows is increased the potential overflow and extent of backwater effects is augmented. Increasing the row spacing between successive rows from 50 mm (test H15_R2_L5) to 100 mm (test H15_R2_L10) leads to a negligible difference in upstream flow depth behavior. Greater backwater effects characterize thicker upstream flow depths which lead to smaller Froude numbers and a higher likelihood that more debris is stagnant upstream of the baffles.

### *Energy loss*

Figure 14 shows a comparison of energy loss profiles for 1.5*h* baffles and the influence of varying row arrangements. The number of rows is increased from a single row array to a three row array, and the spacing between successive rows for two row arrays are varied as 50 mm and 100 mm. Moreover, the control test (H0_R0) is shown as reference. The addition of a second staggered row (test H15_R2_L10) with 100 mm spacing exhibits up to about 40% additional energy loss compared to a single row array (test H15_R1) if transient state energy losses are compared. Adopting a third staggered row (test H15_R2) placed 100 mm from the second row provides up to an additional 32% energy loss during the transient regime. It is evident that increasing the number of rows of 1.5 *h* baffles beyond a single row is effective for impeding mobility. Varying the row spacing for two row arrays from 50 mm (test H15_R2_L5) to 100 mm (test H15_R2_L10) reveals up to an additional 14% energy loss during the transient regime. The function of baffles is to perturb the flow pattern such that flow slows down as it approaches each block and then accelerates as it passes each block and impacts the next row (USFHA 2006). Another benefit of additional staggered rows is to intercept the jets discharging from the slits of the first row of baffles. The impact jet streams against a second staggered row and the further division of jets is one of the contributing interaction mechanisms for energy loss (see Fig. 9*c*). Furthermore, increasing the number of rows of baffles

**Fig. 13.** Comparison of upstream flow depth profiles and row number.

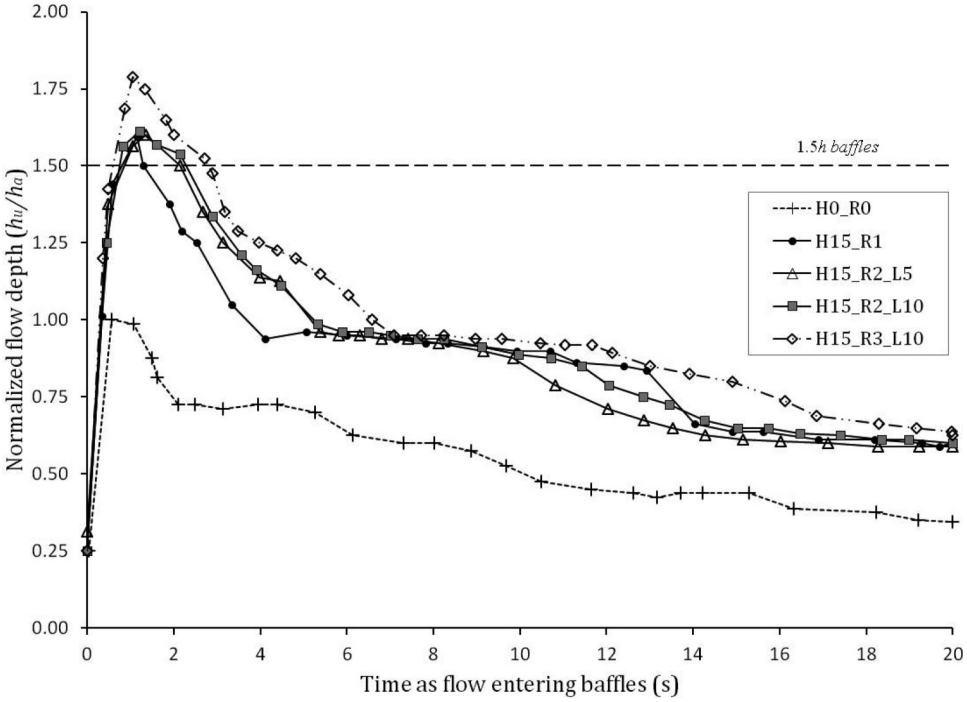


**Fig. 14.** Comparison of row number and spacing between rows.

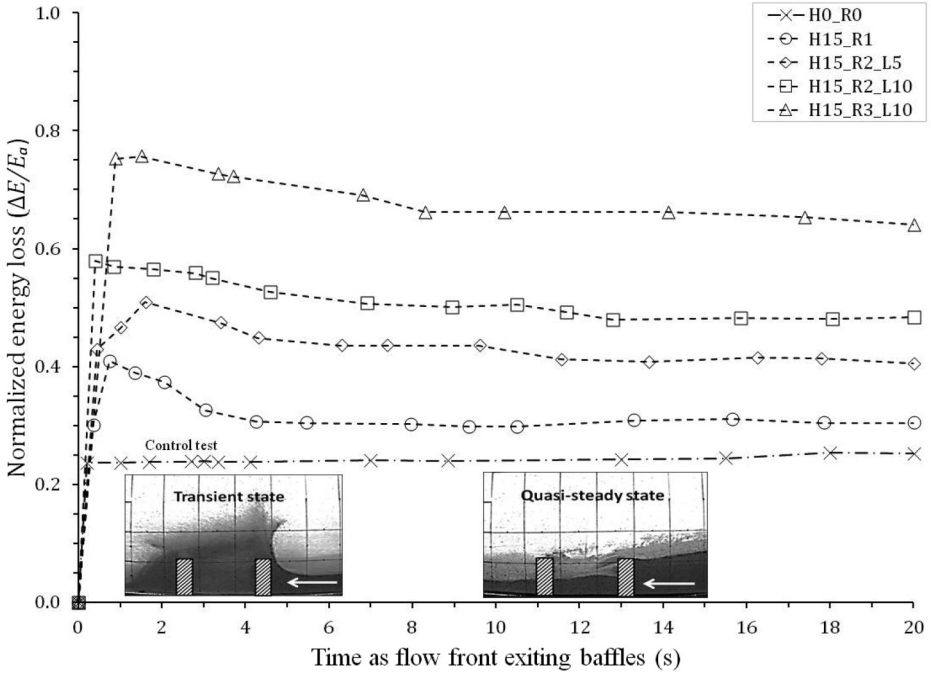


may promote the deposition of sand behind obstacles, which may affect the impedance (Chu et al. 1995; Gray et al. 2003).

Salm (1987) reports that energy dissipation from obstacles is proportional to half the fraction of blockage. The peak flow depth is adopted as the channel depth to approximate the energy dissipation based on the empirical relationship. For short baffles (0.75 *h*), the relationship estimates an energy dissipation of 8% for one row, 16% for two rows, and 23% for three rows. For tall baffles (1.5*h*), the relationship estimates an energy dissipation of 14% for one row, 28% for two rows, and 42% for three rows. The empirical recommendation has no theoretical basis and only considers the upstream surface area of obstruction relative to the channel cross sectional area to contribute to the impedance. The relevancy of this empirical criterion is unclear as the position downstream from the obstacles and the point of measurement during the flow process has not been dictated.

It is recommended by Hákonardóttir et al. (2001) that the first row of obstacles for much shallower and higher supercritical flows ($Fr \approx 10$) reduces flow energy by 20%, and a second staggered row reduces an additional 10%. In other words, two rows of obsta-

cles should yield a 30% energy loss. The recommended individual obstacle geometry from their study is two times the height of the dense core with an aspect ratio of unity above the free surface. If quasi-steady state energy loss values are adopted from this study for comparison, two rows of 1.5*h* baffles spaced 100 mm apart (test H15_R2_L10) adopted in this study yield about 23% energy loss. This energy loss is quite substantial compared to snow avalanche breaking mounds considering the baffle height from this study is 0.5 times shorter and 8 times narrower than the recommended height and width for avalanche obstacles. The effectiveness of the compact baffles used in this study may be attributed to the lower supercritical flow ($Fr \approx 3$) engaged by the baffles compared to the much higher supercritical flows characterizing that of avalanche flows ($Fr \approx 10$).

## Conclusion

An experimental investigation of landslide debris–resisting baffles was carried out. Key flow kinematics during interaction between landslide debris and an array of baffles were described and discussed. The influence of varying baffle height, longitudinal spacing between successive rows, and the number of rows on flow impedance were examined. Conclusions and findings from the results of this study may be drawn as follows:

1. Increasing baffle heights from 0.75*h* to 1.5*h* leads to a 40% increase in upstream flow depth. The upstream flow depths from this study are not easily characterized by theory from hydraulic engineering due to the development of dead zones immediately upstream of the baffles.
2. Increasing baffle heights from 0.75*h* to 1.5*h* leads to more effective development of subcritical conditions. The development of subcritical conditions helps contribute to additional energy losses upstream of the baffles through the potential formation of a granular jump.
3. Increasing baffle heights from 0.75*h* to 1.5*h* leads to additional energy losses of 7% and 9% during the transient state. Energy losses are not observed as the flow depth recedes below 0.75*h*. The energy loss is attributed to the dissipation of potential and kinetic energy through the suppression of runup along a taller baffle face, diminished backwater effects, and potential upstream granular jump.
4. Increasing the number of rows of 1.5*h* baffles from a single row to a three row staggered array leads to up to 72% additional energy loss. Energy loss is attributed to the deflection of granular jets.
5. Increasing the row spacing from 50 to 100 mm leads to an additional 14% energy loss for two staggered rows of 1.5*h* baffles.

## Acknowledgements

The authors would like to acknowledge the financial support from research grant HKUST6/CRF/12R provided by the Research Grants Council of the Government of the Hong Kong SAR, China. This paper is published with the permission of the Head of the Geotechnical Engineering Office and the Director of Civil Engineering and Development, Government of the Hong Kong SAR, China.

## References

Arattano, M., and Franzi, L. 2003. On the evaluation of debris flows dynamics by means of mathematical models. Natural Hazards and Earth System Science, **3**(6): 539–544.

Arattano, M., Deganutti, A.M., and Marchi, L. 1997. Debris flow monitoring activities in an instrumented watershed on the Italian Alps. *In* Proceedings of the 1st ASCE International Conference on Debris-Flow Hazards Mitigation: Mechanics, Prediction & Assessment, San Francisco, California, 7–9 August 1997. American Society of Civil Engineers, New York. pp. 506–515.

Arattano, M., Marchi, L., and Cavalli, M. 2012. Analysis of debris-flow recordings in an instrumented basin: confirmations and new findings. Natural Hazards and Earth System Sciences, **12**: 679–686. doi:10.5194/nhess-12-679-2012.

Armanini, A., Larcher, M., and Odorizzi, M. 2011. Dynamic impact of a debris flow front against a vertical wall. *In* Proceedings of the 5th International Conference on Debris-Flow Hazards Mitigation: Mechanics, Prediction and Assessment, Padua, Italy. pp. 1041–1049.

Chanson, H. 2004. The hydraulics of open channel flow: an introduction. 2nd ed. Elsevier Butterworth-Heinmann, Oxford.

Chu., T., Hill, G., McClung, D.M., Ngun, R., and Sherkat, R. 1995. Experiments on granular flows to predict avalanche runup. Canadian Geotechnical Journal, **32**(2): 285–295. doi:10.1139/t95-030.

Cui, X., and Gray, J.M.N.T. 2013. Gravity-driven granular free-surface flow around a circular cylinder. Journal of Fluid Mechanics, **720**: 314–337. doi:10.1017/jfm.2013.42.

Cui, X., Gray, J.M.N.T., and Jóhannesson, T. 2007. Deflecting dams and the formation of oblique shocks in snow avalanches at Flateyri, Iceland. Journal of Geophysical Research, **112**(F4): F04012. doi:10.1029/2006JF000712.

Faug., T., Caccamo, P., and Chanut, B. 2012. A scaling law for impact force of a granular avalanche flowing past a wall. Geophysical Research Letters, **39**(23): 1–5. doi:10.1029/2012GL054112.

Favier, L., Daudon, D., Donzé, F., and Mazars, J. 2009. Discrete element modelling to compute drag coefficients of obstacles impacted by granular flows. *In* Proceedings of the International Snow Science Workshop, Davos. pp. 500–504.

Gray, J.M.N.T., and Cui, X. 2007. Weak, strong and detached oblique shocks in gravity-driven granular free-surface flows. Journal of Fluid Mechanics, **579**: 113–136. doi:10.1017/S0022112007004843.

Gray, J.M.N.T., Tai, Y.-C., and Noelle, S. 2003. Shock waves, dead zones and particle-free regions in rapid granular free-surface flows. Journal of Fluid Mechanics, **491**: 161–181. doi:10.1017/S0022112003005317.

Hákonardóttir, K.M., Jóhannesson, T., Tiefenbacher, F., and Kern, M. 2001. A laboratory study of the retarding effect of braking mounds in 3, 6 and 9 m long chutes. Report No. 01007. Reykjavík, Veðurstofa Íslands,

Hákonardóttir, K.M., Jóhannesson, T., Tiefenbacher, F., and Kern, M. 2003*a*. Avalanche braking mound experiments with snow. Report No, 03023. Reykjavík, Veðurstofa Íslands.

Hákonardóttir, K.M., Hogg, A.J., Batey, J., and Woods, A.W. 2003*b*. Flying avalanches. Geophysical Research Letters, **30**(23): 1–4. doi:10.1029/2003GL018172.

Hauksson, S., Pagliardi, M., Barbolini, M., and Jóhannesson, T. 2007. Laboratory measurements of impact forces of supercritical granular flow against mast-like obstacles. Cold Regions Science and Technology, **49**(1): 54–63. doi:10.1016/j.coldregions.2007.01.007.

Ho, K.S.S. 2004. Recent advances in geotechnology for slope stabilization and landslide mitigation – perspective from Hong Kong. *In* Proceedings of the 9th International Symposium on Landslides, Rio de Janeiro, 28 June – 2 July 2004 Taylor and Francis. Vol. 2, pp. 1507–1560.

Hübl, J., Suda, J., Proske, D., Kaitna, R., and Scheidl, C. 2009. Debris flow impact estimation. *In* Proceedings of the 11th International Symposium on Water Management and Hydraulic Engineering, Ohrid, Macedonia, 1–5 September 2009. pp. 137–148.

Hungr, O., Evans, S.G., Bovis, M.J., and Hutchinson, J.N. 2001. A review of the classification of landslides of the flow type. Environment and Engineering Geoscience, **7**(3): 221–238.

Ikeya, H., and Uehara, S. 1980. Experimental study about the sediment control of slit sabo dams. Journal of the Japan Erosion Control Engineering Society, **114**: 37–44. [In Japanese.]

Jain, S.C. 2001. Open-channel flow. John Wiley & Sons, New York.

Jóhannesson, T. 2001. Run-up of two avalanches on the deflecting dams at Flateyri, northwestern Iceland. Annals of Glaciology, **32**(1): 350–354. doi:10.3189/172756401781819382.

Jóhannesson, T., Gauer, P., Issler, D., and Lied, K. 2009. The design of avalanche protection dams recent practical and theoretical developments. European Commission, Belgium.

Ng, C.W.W., Choi, C.E., Kwan, J.H.S., Shiu, H.Y.K., Ho, K.K.S., and Koo, R.C.H. 2012. Flume modelling of debris flow resisting baffles. *In* Proceedings of AGS Seminar on Natural Terrain Hazards Mitigation Measures, Hong Kong, 16 October 2012. AGS. pp. 16–21.

Ng, C.W.W., Choi, C.E., and Law, R.P.H. 2013. Longitudinal spreading of granular flow in trapezoidal channels. Geomorphology, **194**: 84–93. doi:10.1016/j.geomorph.2013.04.016.

Roberson, J.A., Cassidy, J.J., and Chaudhry, M.H. 1997. Hydraulic engineering. Houghton Mifflin Company, Boston, Mass.

Salm, B. 1987. Schnee, Lawinen und Lawinenschutz. Vorlesungsskript, ETH Zurich. [In German.]

Sassa, K., and Wang, G. 2005. Mechanism of landslide-triggered debris flows: liquefaction phenomena due to the undrained loading of torrent deposits. *In* Debris-flow hazards and related phenomena. Springer-Berlin, Heidelberg. pp. 81–104. doi:10.1007/3-540-27129-5_5.

Savage, S.B., and Hutter, K. 1989. The motion of a finite mass of granular material down a rough incline. Journal of Fluid Mechanics, **199**(1): 177–215. doi:10.1017/S0022112089000340.

Teufelsbauer, H., Wang, Y., Pudasaini, S.P., Borja, R.I., and Wu, W. 2011. DEM simulation of impact force exerted by granular flow on rigid structures. Acta Geotechnica, **6**(3): 119–133. doi:10.1007/s11440-011-0140-9.

USBR. 1987. Design of small dams. 3rd ed. United States Bureau of Reclamation (USBR), United States Department of the Interior, Washington, D.C.

USFHA. 2006. Hydraulic design of energy dissipators for culverts and channels. Hydraulic Engineering Circular No. 14, 3rd ed., Report No. FHWA-NHI-06-086. United States Federal Highway Administration (USFHA), Springfield, Va.

Vreman, A., Al-Tarazi, M., Kuipers, J., van Sint Annaland, M., and Bokhove, O. 2007. Supercritical shallow granular flow through a contraction: experiment, theory and simulation. Journal of Fluid Mechanics, **578**: 233–269. doi:10.1017/S0022112007005113.

Watanabe, M., Mizuyama, T., and Uehara, S. 1980. Review of debris flow countermeasure facilities. Journal of the Japan Erosion Control Engineering Society, **115**: 40–45. [In Japanese.]

Zanuttigh, B., and Lamberti, A. 2006. Experimental analysis of the impact of dry avalanches on structures and implications for debris flows. Journal of Hydraulic Research, **44**: 552–534. doi:10.1080/00221686.2006.9521703.

Zhang, S. 1993. A comprehensive approach to the observation and prevention of debris flows in China. Natural Hazards, **7**(1): 1–23. doi:10.1007/BF00595676.